High-pressure Raman spectroscopy of tris(hydroxymethyl)aminomethane

DATASET · JUNE 2014

READS
23

9 AUTHORS, INCLUDING:

Wen-Ming Chien
University of Nevada, Reno
45 PUBLICATIONS **158** CITATIONS
SEE PROFILE

Aaron Covington
University of Nevada, Reno
120 PUBLICATIONS **784** CITATIONS
SEE PROFILE

Russell J Hemley
Carnegie Institution for Science
788 PUBLICATIONS **25,513** CITATIONS
SEE PROFILE

Dhanesh Chandra
University of Nevada, Reno
127 PUBLICATIONS **851** CITATIONS
SEE PROFILE

High-Pressure Raman Spectroscopy of Tris(hydroxymethyl)aminomethane

Erik D. Emmons,[†,‡] Juan C. Fallas,[†] Vamsi K. Kamisetty,[†] Wen-Ming Chien,[†] Aaron M. Covington,[§] Raja S. Chellappa,[∥] Stephen A. Gramsch,[∥] Russell J. Hemley,[∥] and Dhanesh Chandra*[,†]

Division of Materials Science, MS 388, University of Nevada, Reno, Reno, Nevada 89557, Department of Physics and Nevada Terawatt Facility, MS 220, University of Nevada, Reno, Reno, Nevada 89557, and Geophysical Laboratory, Carnegie Institute of Washington, 5251 Broad Branch Road, Washington, DC 20015

Received: September 28, 2009; Revised Manuscript Received: February 21, 2010

High-pressure Raman spectroscopy has been used to study tris(hydroxymethyl)aminomethane ($C(CH_2OH)_3NH_2$, Tris). Molecules with globular shapes such as Tris have been studied thoroughly as a function of temperature and are of fundamental interest because of the presence of thermal transitions from orientational order to disorder. In contrast, relatively little is known about their high-pressure behavior. Diamond anvil cell techniques were used to generate pressures in Tris samples up to ~10 GPa. A phase transition was observed at a pressure of ~2 GPa that exhibited relatively slow kinetics and considerable hysteresis, indicative of a first-order transition. The Raman spectrum becomes significantly more complex in the high-pressure phase, indicating increased correlation splitting and significant enhancement in the intensity of some weak, low-pressure phase Raman-active modes.

Introduction

Alcohol and amine derivatives of neopentane [$C(CH_3)_4$] are globular in shape and thus have received a significant amount of attention due to the presence of thermal transitions from orientationally ordered to disordered phases occurring prior to melting.[1] In the high-temperature solid phase, the centers of mass of the molecules still occupy fixed lattice positions but can reorient as a whole about the central carbon atom to form orientationally disordered (ODIC) crystals.[2] These molecules are nearly spherical in shape and hence reorient relatively easily.[2] Above the transition temperature, these materials are easily plastically deformed and are hence also known as "plastic" crystals.[3] Generally, the change in enthalpy for the solid−solid order−disorder transition is significantly larger than that of the transition between the high-temperature disordered solid phase and the melt.[4] Due to the increased freedom of the molecules to reorient on their lattice sites, the heat capacity is also generally higher in the orientationally disordered phase.[5]

Owing to the presence of these solid−solid phase transitions with large changes in enthalpy, compounds such as tris(hydroxymethyl)aminomethane (Tris) have been examined for their potential application as thermal energy storage materials,[4–7] especially for passive solar heating systems for buildings. Materials with solid−solid transitions have the advantage that it is not necessary to provide for the containment of a liquid,[4] as opposed to other materials considered for thermal energy storage which use solid−liquid transitions that have large heats of fusion. In addition, some types of solid−liquid systems may have other disadvantages such as possible segregation of components.[4] In addition to pure compounds, binary mixtures have been explored as a way to adjust the transition properties.[1,4,8,9]

Although the behavior of these polyalcohol and amine materials as a function of temperature has been studied extensively using techniques such as NMR,[10] X-ray diffraction,[2,11] and vibrational spectroscopy,[4,12] they have received very little attention at high pressures. The main focus of these temperature-dependent studies has been on the orientational order−disorder transition. In alcohol and amine derivatives of neopentane, the main effect of the transition on the vibrational spectra is a significant broadening and loss of resolution of the internal modes, and changes and disruptions of hydrogen bonding.[4,13–15] Other effects are apparent, such as the disappearance of the lattice modes.[13,16] Adding pressure as a variable has proven valuable in understanding other materials with orientationally disordered phases, with a well-known example being H_2O.[17]

The polyalcohol pentaerythritol [$C(CH_2OH)_4$], however, has been studied at high pressures by Raman spectroscopy,[18–20] X-ray diffraction,[19] and IR absorption spectroscopy.[21] Evidence was found for two phase transitions at pressures <10 GPa, although there is some discrepancy between the different studies, possibly due to the varying presence or absence of hydrostatic pressure media.[18–20] Under hydrostatic conditions, at ~4.8 GPa, the ambient pressure body-centered tetragonal phase (space group $Pnn2$, $Z = 1$) transforms to an orthorhombic phase (space group $I4$, $Z = 2$).[18,19] In this phase, extensive band doubling was observed due to correlation splitting and a decrease of the molecular symmetry from S_4 to C_2. Another phase was found at pressures >7.2 GPa.[18,19] Evidence was found in the form of line broadening of the Raman bands and X-ray diffraction peaks that above 7.2 GPa pentaerythritol has a disordered structure. An interesting outstanding issue is whether or not high pressure will generally lead to disorder in plastic crystal materials, as high temperature does. In addition to the experimental studies, *ab initio* density functional theory calculations of the vibrational frequency shifts as a function of pressure were performed for pentaerythritol.[22] These studies were motivated both by funda-

* Corresponding author. E-mail: dchandra@unr.edu. Phone: (775) 784-6771. Fax: (775) 327-5059.
† Division of Materials Science, University of Nevada.
‡ Current address: U.S. Army Edgewood Chemical Biological Center, Research and Technology Directorate, 5183 Blackhawk Road, RDCB-DRD-L/BLDG E5560, Aberdeen Proving Ground, MD 21040.
§ Department of Physics and Nevada Terawatt Facility, University of Nevada.
∥ Carnegie Institute of Washington.

10.1021/jp9092892
Published on Web 04/13/2010

mental scientific interest in pentaerythritol and by applications of the related explosive material pentaerythritol tetranitrate. Pentaerythritol tetranitrate under high pressure has been examined both with *ab initio* theoretical calculations[23] and experimentally under static[24] and dynamic[25] compression. Evidence was found in the experimental studies for a phase transition at 4 GPa involving conformational changes.

There have been a few other studies of polyalcohols at high pressures. For example, Rittmeier-Kettner and Schneider[26] determined the *PT* phase diagram for neopentylglycol (NPG, $C(CH_3)_2(CH_2OH)_2$), for 0 GPa < *P* < 0.7 GPa and 300 K < *T* < 375 K, in the range where the phase line between the orientationally ordered and disordered phases is present, using differential thermal analysis (DTA). Three different phases are present in this region. The transition to an orientationally disordered phase is observed at 315 K in NPG at atmospheric pressure. Application of pressure at room temperature leads to a first-order transition at ~0.42 GPa. This high-pressure phase, which is distinct from the high-temperature orientationally disordered phase, is the same phase that was observed at low temperature (*T* ~60 K) at ambient pressures by Kamae et al.[3] Rittmeier-Kettner et al. claim this based on an extrapolation of their phase diagram to lower temperatures.[26] A triple point was observed at 363 K and 0.646 GPa.

In this study, Raman spectroscopy is used to study tris(hydroxymethyl)aminomethane ($C(CH_2OH)_3NH_2$, hereafter denoted simply as Tris) at high pressures inside a diamond anvil cell (DAC). In the solid state under ambient conditions (*P* = 1 bar, *T* = 298 K), a single Tris molecule lacks any symmetry.[27] Hence, all of the internal vibrational modes are active in both the infrared and Raman spectra. There are relatively few vibrational spectroscopy studies of Tris; however, Schroetter and Bougeard identified the bands in the infrared and Raman spectra using a normal coordinate analysis for an isolated Tris molecule.[28] In addition, Schroetter and Bougeard,[13] as well as Kanesaka and Mizuguchi,[12] studied the vibrational spectra of Tris as a function of temperature. Vibrational spectroscopy studies of other closely related polyalcohols such as pentaerythritol are also helpful for identifying the analogous spectral modes in Tris.[29,30]

Under ambient conditions, the crystal structure of Tris adopts the orthorhombic $Pn2_1a$ space group with four molecules per unit cell.[2] Many polyalcohols and amines such as Tris form layered structures perpendicular to the *c*-axis with strong intralayer hydrogen bonds and relatively weak interlayer hydrogen bonds. In the case of Tris, the amino groups are oriented along the *c*-axis,[12] and are involved only weakly in hydrogen bonding. Kanesaka and Mizuguchi found that the structure of Tris may be more accurately modeled as a chain structure, where the hydrogen bonds are stronger along the *b*-axis than the *a*-axis.[12] Evidence for this was seen in the observed doublet correlation splitting of several modes in the infrared spectrum. Above 407 K, the structure changes to the body-centered-cubic $Im3m$ space group with two molecules per unit cell and orientational disorder.[2] In addition, evidence for another first-order phase transition was found by Kanesaka and Mizuguchi at 190 K.[12] The molecular and crystalline structure of Tris in the ambient phase are shown in Figure 1.

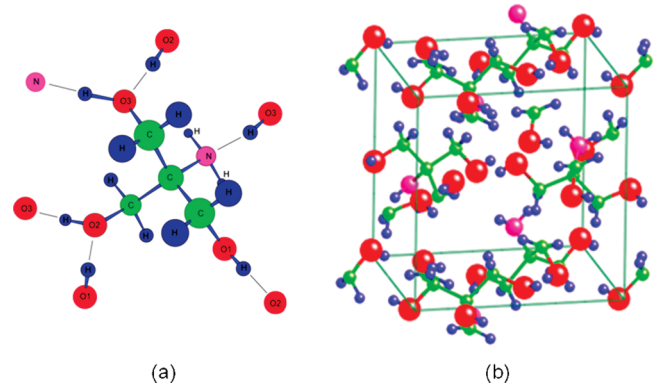

Figure 1. (a) Ambient temperature and pressure conformation of a single Tris molecule in the solid state. The black lines indicate hydrogen bonds with adjacent molecules. (b) Crystal structure of Tris in the ambient pressure orthorhombic $Pn2_1a$ phase.

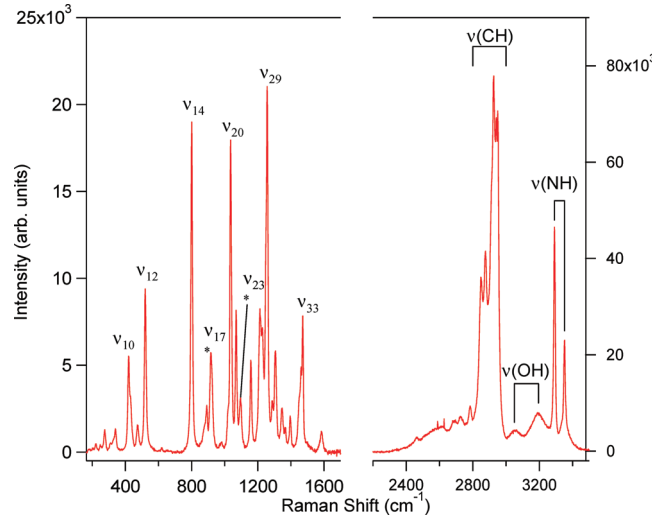

Figure 2. Ambient temperature and pressure Raman spectrum of a bulk sample of Tris. The left-hand side of the figure shows the low-frequency deformation modes, while the right-hand side of the figure shows the CH, OH, and NH stretching modes. The more intense modes are labeled (see Table 1), and modes that could not be identified to be associated with a particular type of molecular motion are indicated with asterisks.

Experimental Technique

A four-post high-pressure diamond anvil cell (DAC) (High Pressure Diamond Optics, Tucson, AZ) with 0.6 mm culet diamonds was used to perform the Raman spectroscopy studies.[31–33] Type I diamonds selected for low fluorescence were used in order to minimize the background level in the Raman spectra. Inconel gaskets of initial 250 μm thickness were preindented and drilled with holes of diameter ranging from 170 to 250 μm. These holes served as sample chambers. The standard ruby fluorescence technique was used to calibrate the pressure. The measurements were repeated to check for consistency.

High-purity Tris (Alfa-Aesar, >99.8% purity) that was finely ground with a mortar and pestle was used. No pressure medium was used, since these materials are typically quite soft. Raman spectroscopy was performed using a Renishaw InVia Raman microscope. An argon ion laser tuned to the 514.5 nm line was used to excite the sample. Typically, ~5−7 mW of laser power was incident upon the DAC. The laser beam was focused on the sample using a 20× microobjective (0.40 N.A.). Raman scattered light was collected in the backscattering geometry, and notch filters were used to filter out the Rayleigh scattered light. An 1800 grooves/mm diffraction grating was used to disperse the Raman scattered light, which was then incident on a thermoelectrically cooled (−70 °C) CCD camera (Renishaw

TABLE 1: List of Vibrational Mode Frequencies and Assignments of Internal Modes of Tris[a]

label	current frequencies (cm^{-1})	Schroetter[28] frequency (cm^{-1})	assignment and % PED
ν_3	221.8		CC twist (skeletal)
ν_4	250.1		τ(CCO)
ν_5	275.4		τ(CCO)
ν_6	308.7	311 (IR)	δ(CCC)-62%
	329.1	330 (IR)	τ(CN)-90%
ν_7	341.0	342	τ(CN)-90%
ν_{10}	419.7	420 (IR)	δ(NCC)-42%
		424	δ(CCC)-20%
	431.8	420 (IR)	δ(NCC)-42%
		424	δ(CCC)-20%
ν_{11}	474.2	470 (IR)	δ (NCC)-63%
		476	
ν_{12}	520.3	524	δ(NCC)-49%
		530 (IR)	δ(HCC)-21%
ν_{13}	620.0	633 (IR)	δ(CCC)
		655 (IR)	τ(CO)
		715 (IR)	τ(CO)
		790 (IR)	δ(HNC)-54%
ν_{14}	800.6	804	ν(CC)
ν_{15}	878.5	875	δ(HCC)-45%
			τ(CO)-27%
ν_{16}	891.6	896	δ(HCC)-41%
			δ(HNC)-22%
ν_{17}	918.1	917	?
		925 (IR)	δ(HCC)-57%
			τ(CO)-21%
ν_{18}	980.3	983 (IR)	δ(HNC)-43%
			ν(CC)-27%
ν_{19}	1018.2	1024	ν(CO)-67%
ν_{20}	1036.3	1049	ν(CO)-60%
ν_{21}	1069.3	1071	ν(CO)-60%
ν_{23}	1095.6	1098	?
ν_{25}	1158.1	1161	δ(HNC)-34%
ν_{27}	1211.8	1215	δ(OH)-42%
			δ(HCO)-23%
ν_{28}	1227.6	1230	δ(HCO)-43%
			δ(OH)-25%
ν_{29}	1255.7	1259	ν(CC)-27%
	1286.7	1292	δ(OH)-39%
			δ(HCO)-39%
	1306.3	1306	δ(OH)-37%
			δ(HCO)-30%
	1345.7	1346	δ(OH)-30%
			δ(HCC)-27%
	1366.6	1373	δ(HCC)-33%
			ν(CC)-23%
ν_{30}	1396.0	1400	ν(CC)-37%
			δ(HCC)-26%
ν_{31}	1450.9	1452	$\delta(CH_2)$-58%
			δ(HCO)-38%
ν_{32}	1461.5	1464	$\delta(CH_2)$-58%
			δ(HCO)-38%
ν_{33}	1471.6	1474	$\delta(CH_2)$-60%
			δ(HCO)-37%
		1493 (IR)	?
ν_{34}	1584.6	1590	$\delta(NH_2)$-87%
	2848.8		$\nu_s(CH_2)$
	2876.0		$\nu_s(CH_2)$
	2925.7		$\nu_a(CH_2)$
	2939.9		$\nu_a(CH_2)$
	2951.6		$\nu_a(CH_2)$
	3049.8		ν(OH)
	3194.7		ν(OH)
ν_{NH1}	3291.0	3295	$\nu_s(NH_2)$
	3331.5	3335	ν(OH)
ν_{NH2}	3351.2	3355	$\nu_a(NH_2)$

[a] The bands at frequencies below 300 cm^{-1} were identified by analogy with pentaerythritol.[29,30] For the peaks with frequencies greater than 300 cm^{-1}, the assignments and potential energy distributions (% PED) are based on the normal mode calculations of Schroetter and Bougeard,[28] except for a few cases where those of Kanesaka and Mizuguchi[12] were preferred. The mode frequencies are compared to those of Schroetter and Bougeard. In a few cases, Schroetter and Bougeard only observed a band in the IR spectrum corresponding to a peak observed here in the Raman spectrum. The labels correspond to the modes as listed in Table 2, which gives their pressure-induced frequency shifts. An unlabeled mode indicates that it was not observable in either the low- or high-pressure phases in the DAC but was observable in a bulk sample in the infrared or Raman spectrum.

TABLE 2: Pressure-Induced Frequency Shifts for the Deformation Modes of the α- and β-Phases of Tris[a]

mode and ambient frequency (α-phase, cm^{-1})	mode and ambient frequency (β-phase, cm^{-1})	$d\nu/dp$ (α-phase) (cm^{-1}/GPa)	$d\nu/dp$ (β-phase) (cm^{-1}/GPa)
	ν_1 (146.6)		6.5
	ν_2 (195.6)		3.6
ν_3 (221.8)	ν_3 (213.0)	7.6	9.5
ν_4 (250.1)	ν_4 (248.6)		6.4
ν_5 (275.4)	ν_5 (279.1)	6.5	7.5
ν_6 (308.7)	ν_6 (299.6)		9.1
ν_7 (339.0)	ν_7 (339.7)	8.7	7.2
	ν_8 (379.2)		3.5
	ν_9 (380.3)		10.7
ν_{10} (419.7)	ν_{10} (430.4)	6.4	4.6
ν_{11} (474.2)	ν_{11} (471.1)	8.0	7.5
ν_{12} (520.3)	ν_{12} (537.6)	7.5	5.0
ν_{13} (620.0)	ν_{13} (635.1)		3.8
ν_{14} (800.7)	ν_{14} (779.4)	9.3	6.0
ν_{15} (878.5)	ν_{15} (878.7)		4.0
ν_{16} (891.6)	ν_{16} (889.6)	8.0	5.4
ν_{17} (918.1)	ν_{17} (903.5)	3.6	4.8
ν_{18} (980.3)	ν_{18} (957.7)		5.7
ν_{19}(1018.2)	ν_{19}(1006.6)	4.1	5.6
ν_{20}(1036.3)	ν_{20}(1040.4)	7.0	4.0
	ν_{21}(1039.0)		7.0
ν_{22}(1069.3)	ν_{22}(1076.6)	5.2	5.8
ν_{23}(1096.2)		10.3	
	ν_{24}(1137.3)		4.9
ν_{25}(1158.1)	ν_{25}(1158.6)	3.4	4.3
	ν_{26}(1173.5)		4.3
ν_{27}(1211.8)	ν_{27}(1205.8)	7.6	3.8
ν_{28}(1227.6)	ν_{28}(1233.6)	7.3	4.3
ν_{29}(1255.7)	ν_{29}(1251.4)	4.4	4.2
ν_{30}(1396.0)	ν_{30}(1396.0)	4.8	5.7
ν_{31}(1450.9)	ν_{31}(1443.3)		1.9
ν_{32}(1461.5)	ν_{32}(1454.9)		2.2
ν_{33}(1471.6)	ν_{33}(1465.7)	2.0	2.8
ν_{34}(1584.6)	ν_{34}(1601.4)	4.9	1.2
	ν_{35}(1617.1)		4.7

[a] Linear fits were used based on data acquired during pressure increase. For the β-phase, the "ambient frequencies" indicate the intercept of the linear fit with the $p = 0$ axis. In the first column, unlabeled frequencies indicate that a mode was observable in a bulk sample in the infrared or Raman spectra but not in the Raman spectrum of the low-pressure phase in the DAC. Several modes could be tracked only in the high-pressure phase. In addition, one mode (ν_{24}) could be tracked in the low-pressure phase but not in the high-pressure phase.

RenCam CCD). The spectrometer entrance slit was set at a width of ~50 μm, leading to a spectral resolution of ~4−5 cm^{-1}.

Results

The Raman spectra of Tris under ambient conditions are shown in Figure 2. Since an isolated Tris molecule lacks any symmetry, all of the vibrational modes are expected to be both infrared- and Raman-active. Some modes, however, were unobservably weak in either the Raman spectrum or the infrared spectrum. A list of the mode frequencies and description of the atomic motions involved is given in Table 1. The mode assignments for bands at frequencies lower than 300 cm^{-1} were obtained by analogy with pentaerythritol.[29,30] The mode assignments for bands at frequencies higher than 300 cm^{-1} were taken from Schroetter and Bougeard,[28] with the exception of the CH stretching modes, which were not assigned in that work, and a few cases where the assignments of Kanesaka and Mizuguchi[12] were taken instead, since they were judged to be a more accurate description of the modes. The normal coordinate analysis of Schroetter and Bougeard indicates that most of the vibrational modes cannot be described simply but rather are mixtures of different types of motions.

Evidence for a phase transition in Tris is shown in the Raman spectra in Figure 3. At ambient temperature, spectra are shown at pressures of 0.7 and 3.4 GPa and are each of a single phase. The high-pressure phase is denoted here as β-Tris. Many additional peaks are present in the β-phase that were not present in the low-pressure α-phase. For comparison, the orientationally disordered γ-phase is shown as well, at ambient pressure and $T = 135$ °C. The γ-phase is distinctive in the significant band broadening that is observable compared to the α- and β-phases, attributed to variations in the intermolecular force fields experienced by the molecules. The newly observed β-phase is most likely not an orientationally disordered phase, since the bandwidths are more comparable to that of the orientationally ordered α-phase.

Figure 4 shows additional spectra in the region of the CH, OH, and NH stretches, in order to illustrate the evolution of the phase transition. Spectra were measured after increasing and decreasing pressure steps, and demonstrate considerable hysteresis. Approximately 25 min was allowed for the system to evolve after increasing the pressure before beginning a spectral scan. With increasing pressure, indications of the phase transition are shown in the spectra measured at a pressure of 1.9 GPa. For example, the two NH stretching modes begin to show shoulders, indicating a mixture of two phases. After waiting for a further 30 min at the same nearly constant pressure, the shoulders become more prominent, indicating that a larger fraction of the sample had transformed. The OH stretching modes also become more prominent relative to the NH stretching

modes. The temporal evolution of the spectra indicates that the transition is marked by relatively sluggish kinetics. With decreasing pressure, the α-phase was not recovered until the pressure was near ambient, providing further evidence for an energy barrier to the transition. This hysteresis effect is indicative of a first-order phase transition.

The pressure-induced frequency shifts for many of the vibrational modes of Tris were measured. The results are tabulated in Table 2 for the deformation modes of both the low- and high-pressure phases of Tris. Table 3 shows similar coefficients for the OH and NH stretching modes. For the high-pressure phase, it was found that quadratic fits were necessary to adequately fit the data for the NH stretching modes. Here, a quadratic function of the form $\nu(p) = \nu_0 + (d\nu/dp)_0 p + (d^2\nu/dp^2)p^2$ was used to fit the data. The CH stretching modes were not analyzed as a function of pressure.

NH and OH Stretching Modes. Figure 5 shows the pressure-induced frequency shifts for the NH_2 stretching vibrations. In the low-pressure phase, a linear function was suitable to describe the behavior of these modes. In the high-pressure phase, however, it was necessary to use a quadratic function. Quadratic functions have been shown before to be necessary to model the pressure shift of the frequencies for some modes.[31,34] In the low-pressure phase, both modes decrease in frequency as the pressure is increased. This is an indication of the increased importance of intermolecular hydrogen bonding of the NH_2 groups. Above the phase transition, the dependence of the mode frequencies on pressure is more complex, and indicates that the nature of the hydrogen bonds is changing. There is a clear discontinuity in the frequencies at the phase transition, indicating that it is of first order. In addition, for some of the spectra measured near the phase transition, the two phases could be observed to coexist, indicating slow kinetics.

Although the OH stretching modes could not easily be tracked in the low-pressure phase due to their low intensities, three OH stretching modes could be observed and tracked in the high-pressure phase. These modes, which do not have clear counterparts in the low-pressure phase, were interpreted as stretching modes of OH groups involved in hydrogen bonding due to their broad nature. Plots of the Raman shifts as a function of pressure are shown in Figure 6. There is significant scatter in the data. The lowest and highest frequency modes of these three had very small pressure-induced frequency shifts. The mode with a frequency near 3220 cm^{-1} at 2 GPa had a more significant positive slope.

Deformation Modes. Finally, shifts of the low-frequency deformation modes are shown in Figure 7. Not all of the modes could be traced to the highest pressures due to low and decreasing intensities with increasing pressure. Discontinuities in the mode frequencies and $d\nu/dp$ values could be observed for nearly all of the modes at the phase transition, indicating that the transition is of first order. Mode frequencies and $d\nu/dp$ values either decrease or increase, depending on the particular mode. Modes in the vicinity of the 1332 cm^{-1} Raman-active first-order phonon mode of diamond could not be tracked due to the large amount of interference from the diamond feature.

There are several modes of Tris that are difficult to observe in the Raman spectra of the low-pressure phase of the sample in the DAC which become significantly more intense in the high-pressure phase. The τ(CCO) mode at 250.1 cm^{-1} and the δ(CCC) mode at 308.7 cm^{-1} are examples of this phenomena. The clearest example of this is in the τ(CO) torsional modes that were observed by Schroetter and Bougeard at 633 and 655 cm^{-1} in the IR spectrum (the mode at 633 cm^{-1} was attributed primarily to CCC bending motions by Kanesaka and Mizuguchi[12]). In the ambient pressure Raman spectrum, only an extremely weak mode is observable in the Raman spectrum near 620 cm^{-1}. In the high-pressure phase, however, a significantly more intense mode is observed near 640 cm^{-1} at a pressure of

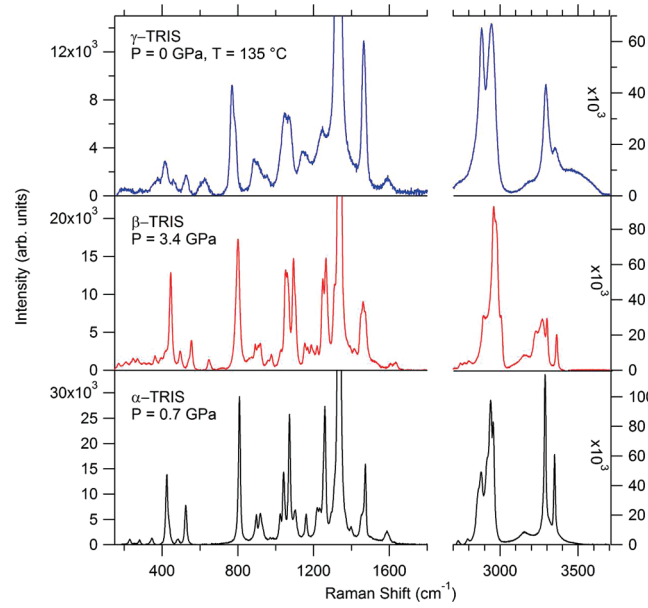

Figure 3. Raman spectra of Tris in the low-pressure α-phase, high-pressure β-phase, and high-temperature γ-phase. The left-hand side of the figure shows the deformation modes, while the right-hand side shows the CH, NH, and OH stretching modes. The strong first-order phonon line from diamond is present at ~1330 cm^{-1} and masks some of the modes in this region.

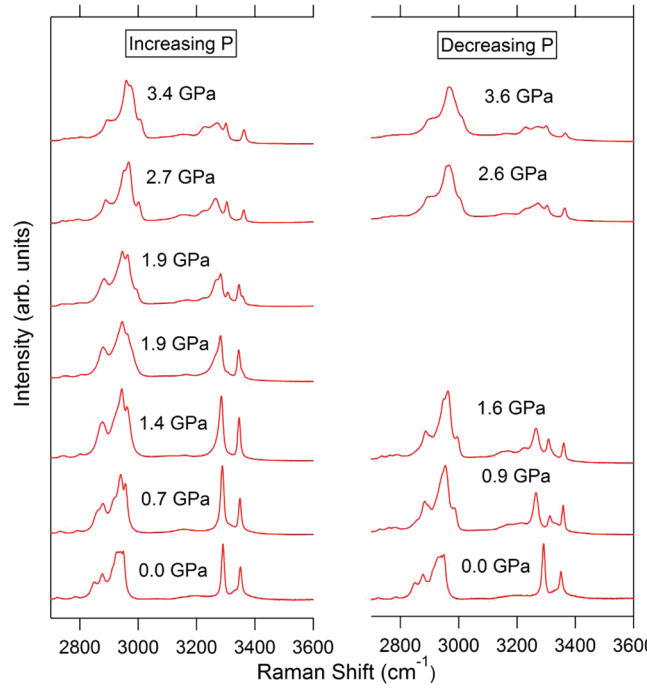

Figure 4. Pressure-dependent Raman spectra of Tris in the region of the C−H stretching (~2800−3000 cm^{-1}), O−H stretching (~3000−3400 cm^{-1}), and N−H stretching (3200−3400 cm^{-1}) vibrations. The spectra on the left side were taken during pressure increase, while those on the right were taken during pressure decrease. The second measurement at 1.9 GPa was taken 30 min after the first one, while the other measurements were taken approximately 25 min after the previous one. Considerable hysteresis is evident, indicative of slow kinetics for the first-order phase transition.

TABLE 3: Pressure-Induced Frequency Shifts of the OH and NH Stretching Modes of the α- and *β*-Phases of Tris[a]

mode (frequency) (α-phase, cm^{-1})	mode (frequency) (*β*-phase, cm^{-1})	$d\nu/dp$ (α-phase) (cm^{-1}/GPa)	$(d\nu/dp)_0$ (*β*-phase) (cm^{-1}/GPa)	$d^2\nu/dp^2$ (*β*-phase) (cm^{-1}/GPa^2)
	ν_{OH1} (3159.9)		0.6 (0.6)	
	ν_{OH2} (3218.0)		2.4 (0.3)	
	ν_{OH2} (3268.6)		−0.4 (0.7)	
ν_{NH1} (3291.0)	ν_{NH1} (3316.8)	−4.18	−5.88	0.393
ν_{NH2} (3351.2)	ν_{NH2} (3351.3)	−2.92	5.12	−0.422

[a] The three OH stretching modes could only be traced in the high-pressure phase due to low intensities in the low-pressure phase. In the high-pressure phase, it was necessary to use quadratic functions to accurately model the frequency shifts of the NH stretching modes. Errors in the linear fits for the OH stretching modes are shown in parentheses, and are very large for the ν_{OH1} and ν_{OH3} modes, due to significant scatter in the data.

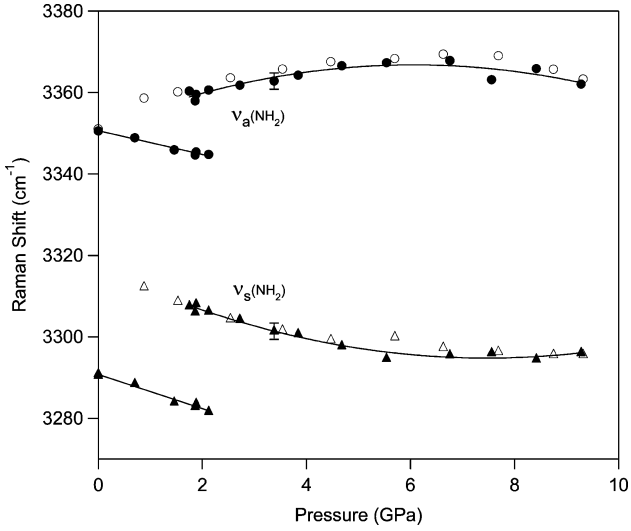

Figure 5. Raman shift as a function of pressure for the symmetric (triangles, denoted $\nu_s(NH_2)$) and asymmetric (circles, denoted $\nu_a(NH_2)$) NH_2 stretching modes of Tris. The solid symbols were obtained upon pressure increase, while the open symbols were obtained upon pressure decrease. Linear fits were performed for the low-pressure phase, while quadratic fits were performed for the high-pressure phase. These fits used only the data obtained upon pressure increase.

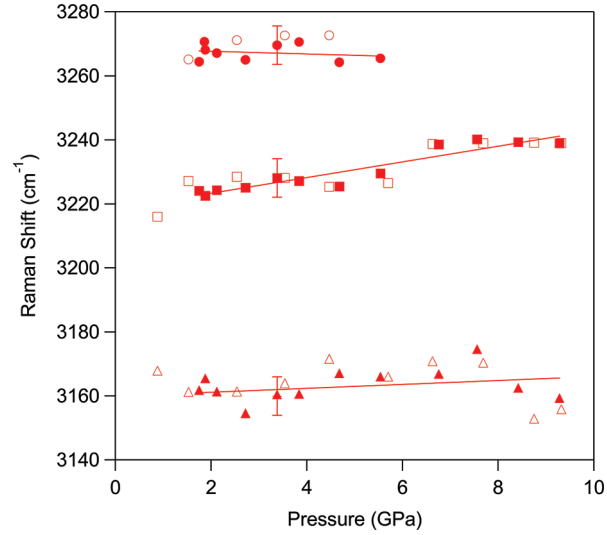

Figure 6. Pressure-induced frequency shifts of three OH stretching modes in the high-pressure phase, denoted by circles, squares, and triangles, from highest to lowest frequency. The solid symbols indicate data acquired during pressure increase, while the open symbols indicate data acquired during pressure decrease. The OH stretching modes were difficult to track at low pressures due to their low intensities but became more intense relative to the CH and NH stretching modes at high pressures. These fits were performed with data obtained only during pressure increase. Representative error bars are shown.

1.9 GPa. Note that these modes become easily observable in the ODIC *γ*-phase as well.

The *δ*(HNC) mode at 1158.1 cm^{-1} appears to split into a triplet of peaks as a result of the phase transition. There are no other nearby peaks in the infrared spectra that are not observable in the Raman spectrum, so it appears that the effect may be the result of increased correlation splitting at higher pressures. It is also possible that modes near these frequencies that are weak in both the infrared and Raman spectra become observable in the high-pressure phase.

The three mixed $\delta(CH_2)/\delta(HCO)$ scissoring modes in the range 1450−1472 cm^{-1} show significant changes in relative intensities above the phase transition. Only the strongest of the three modes at 1472 cm^{-1} could be tracked in the low-pressure phase; the other two peaks were weak and unresolved in the DAC. In the high-pressure phase, however, all three modes could be partially resolved and the relative intensities became more comparable. As a result, it was possible to track the mode frequencies as a function of pressure.

The $\delta(NH_2)$ scissoring mode at 1585 cm^{-1} shows interesting behavior as a result of the phase transition. It splits into a clearly observable doublet in the high-pressure phase, possibly as a result of increased correlation splitting. The pressure-induced frequency shifts of these two modes are significantly different, with the higher frequency mode shifting at a much faster rate. In addition, the frequency versus pressure plots tend to flatten out above ∼4 GPa. A similar change in slope was observed for the $\nu(NH_2)$ stretching modes, which is likely the result of changing hydrogen bond interactions.

Discussion

There is a significant increase in the number of the internal modes of Tris above the pressure-induced phase transition. Two factors contribute to this observed effect. First, there are several modes of the ambient pressure phase that, while being strictly considered active in Raman scattering due to the lack of symmetry of the isolated Tris molecule, are extremely weak. Many of these modes can be observed more easily in the infrared spectrum at ambient pressure. After the phase transition, many of these modes become significantly more intense due to changes in the crystal structure and/or possible conformational changes in the individual Tris molecules. A similar effect was also observed in the high-pressure Raman spectroscopy study of pentaerythritol ($C(CH_2OH)_4$) by Park et al.[18] In that study, some CCO twisting and bending modes could not be tracked in the ambient pressure phase in the diamond cell. A decrease in the molecular symmetry from S_4 to C_2 and a change in the crystal lattice structure at the phase transition in general could lead to an increase in intensity of some of the weak modes of

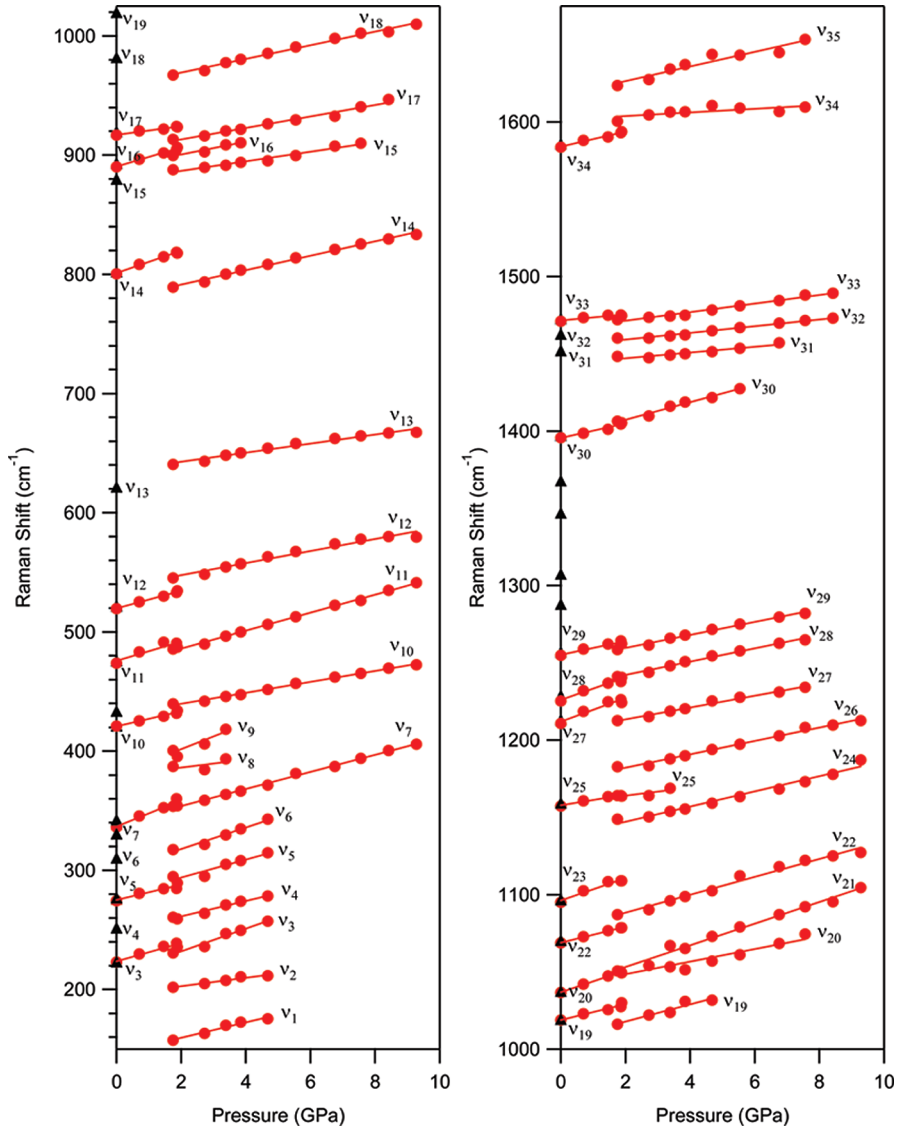

Figure 7. Pressure-induced frequency shifts of the low-frequency deformation modes of Tris. Discontinuities and changes in slope can be observed above the phase transition. In addition, new modes can be tracked in the high-pressure phase that were difficult or impossible to observe in the low-pressure phase. Some of the lower intensity modes in the high-pressure phase could not be tracked to the highest pressures due to poor statistics. The black triangles indicate modes observed under ambient conditions in a bulk sample in the infrared or Raman spectra. Some of these modes could not be observed in the DAC due to the small sample size. The labels indicate the mode identifications indicated in Table 1. The error bars are generally smaller than the points.

pentaerythritol. A change in the molecular conformation and/or crystal structure also appears to be causing a similar effect in Tris.

The second likely cause of the increased number of modes observable in the high-pressure phase is increased intermolecular interactions, which leads to more easily observed correlation splitting in the high-pressure phase. For the ambient pressure orthorhombic $Pn2_1a$ phase, there are four molecules per unit cell.[2] Hence, each internal mode is split into four modes in the crystal. However, for all of the modes, only one or two components are resolved in the ambient α-phase. The doublet structure of many of the peaks was attributed by Kanesaka and Mizuguchi to the chain structure in crystalline Tris, in which the strongest intermolecular hydrogen-bonding interactions are along the crystal *b*-axis.[12] Although high-pressure X-ray diffraction measurements would be necessary in order to determine the detailed structure of the high-pressure phase, certain aspects of the structure can be determined from the Raman spectra. It is likely that the high-pressure phase still contains more than one molecule per unit cell, which helps to explain the large number of peaks present in the high-pressure phase. Additional measurements would clearly be helpful in this regard in order to elucidate the fundamental behavior of Tris at the conditions that lead to this phase transition. Further temperature- and pressure-dependent X-ray diffraction, infrared absorption, and Raman scattering measurements would be very valuable, and would work together synergistically to determine more information about the structure of the system. In particular, high-pressure X-ray diffraction would be useful for gaining a better understanding of hydrogen bonding in the high-pressure phase of Tris.

Conclusions

Raman spectroscopy was used to study tris(hydroxymethyl)aminomethane at high pressures inside a diamond anvil cell. A phase transition was observed at ~2 GPa. In addition to discontinuous changes in many of the mode frequencies and slopes of the frequency versus pressure curves above this phase

transition, new modes were present that were difficult to observe or not present in the low-temperature phase. This indicates a significant change in the crystal lattice structure and/or the molecular conformations in the material. The phase transition is marked by slow kinetics and significant hysteresis, indicative of a first-order process.

Further work is underway to measure the Raman spectra of Tris as a function of pressure *and* temperature in order to obtain the *PT* phase diagram. In addition, other polyalcohol and amine derivatives of neopentane are being examined to order see how pressure affects the properties of these plastic crystal materials with globular molecules. Of particular interest is the effect of pressure on the orientational-disorder transitions present in these systems. These measurements are important both from a fundamental scientific viewpoint and for applications of these materials, such as use as thermal energy storage materials.

Acknowledgment. This work was supported by the U.S. DOE through the Carnegie-DOE Alliance Center (CDAC) grant DE-FC-03-03NA00144 as an academic partner. Support for A.M.C. and spectroscopy equipment at the Optical Properties of Materials laboratory at UNR was also provided by the U.S. DOE through grant DE-FC52-06NA27616. J.C.F. acknowledges a scholarship from the Science and Technology Ministry of Costa Rica (MICIT) and National Council for Scientific and Technological Research of Costa Rica (CONICIT).

References and Notes

(1) Chellappa, R.; Chandra, D. *CALPHAD: Comput. Coupling Phase Diagrams Thermochem.* **2003**, *27*, 133–140.
(2) Eilerman, D.; Rudman, R. *J. Chem. Phys.* **1980**, *72*, 5656–5666.
(3) Kamae, R.; Suenaga, K.; Matsuo, T.; Suga, H. *J. Chem. Thermodyn.* **2001**, *33*, 471–484.
(4) Benson, D. K.; Burrows, R. W.; Webb, J. D. *Sol. Energy Mater.* **1986**, *13*, 133–152.
(5) Divi, S.; Chellappa, R.; Chandra, D. *J. Chem. Thermodyn.* **2006**, *38*, 1312–1326.
(6) Chandra, D.; Chien, W. M.; Gandikotta, V.; Lindle, D. W. *Z. Phys. Chem.* (Muenchen, Ger.) **2002**, *216*, 1433−1444.
(7) Chandra, D.; Mandalia, H.; Chien, W. M.; Lindle, D. W.; Rudman, R. *Z. Phys. Chem.* (Muenchen, Ger.) **2002**, *216*, 1389−1400.
(8) Chellappa, R.; Russell, R.; Chandra, D. *CALPHAD: Comput. Coupling Phase Diagrams Thermochem.* **2004**, *28*, 3–8.
(9) Russell, R.; Chellappa, R.; Chandra, D. *Calphad-Computer Coupling of Phase Diagrams and Thermochemistry* **2004**, *28*, 41–48.
(10) Wasylishen, R. E.; Barron, P. F.; Doddrell, D. M. *Aust. J. Chem.* **1979**, *32*, 905–909.
(11) Rudman, R.; Eilerman, D.; Laplaca, S. J. *Science* **1978**, *200*, 531–533.
(12) Kanesaka, I.; Mizuguchi, K. *J. Raman Spectrosc.* **1998**, *29*, 813–817.
(13) Schroetter, S.; Bougeard, D. In *Dynamics of Molecular Crystals*; Lascombe, J., Ed.; Elsevier: Grenoble, France, 1986; pp 213−218.
(14) Granzow, B. *J. Mol. Struct.* **1996**, *381*, 127–131.
(15) Granzow, B.; Klaeboe, P.; Sablinskas, V. *J. Mol. Struct.* **1995**, *349*, 153–156.
(16) Woost, B.; Bougeard, D. *J. Chem. Phys.* **1986**, *84*, 4810–4817.
(17) Song, M.; Yamawaki, H.; Fujihisa, H.; Sakashita, M.; Aoki, K. *Phys. Rev. B* **2003**, *68*, 024108.
(18) Park, T. R.; Dreger, Z. A.; Gupta, Y. M. *J. Phys. Chem. B* **2004**, *108*, 3174–3184.
(19) Dreger, Z. A.; Gupta, Y. M.; Yoo, C. S.; Cynn, H. *J. Phys. Chem. B* **2005**, *109*, 22581–22587.
(20) Bhattacharya, T.; Sharma, S. M. *J. Phys.: Condens. Matter* **2002**, *14*, 10367–10375.
(21) Deb, S. K.; Banerji, A.; Kshirsagar, R. J.; Sharma, S. M.; Dumas, P.; Marin, T.; Chervin, J. C.; Canny, B. *Infrared Phys. Technol.* **2006**, *49*, 82–87.
(22) Perger, W. F.; Vutukuri, S.; Dreger, Z. A.; Gupta, Y. M.; Flurchick, K. *Chem. Phys. Lett.* **2006**, *422*, 397–401.
(23) Perger, W. F.; Zhao, J. J.; Winey, J. M.; Gupta, Y. M. *Chem. Phys. Lett.* **2006**, *428*, 394–399.
(24) Gruzdkov, Y. A.; Dreger, Z. A.; Gupta, Y. M. *J. Phys. Chem. A* **2004**, *108*, 6216–6221.
(25) Hemmi, N.; Dreger, Z. A.; Gruzdkov, Y. A.; Winey, J. M.; Gupta, Y. M. *J. Phys. Chem. B* **2006**, *110*, 20948–20953.
(26) Rittmeier-Kettner, M.; Schneider, G. M. *Thermochim. Acta* **1995**, *266*, 185–187.
(27) Golovina, N. I.; Raevskii, A. V.; Fedorov, B. S.; Chukanov, N. V.; Shilov, G. V.; Leonova, L. S.; Tarasov, V. P.; Erofeev, L. N. *J. Solid State Chem.* **2002**, *164*, 301–312.
(28) Schroetter, S.; Bougeard, D. *Ber. Bunsen-Ges.* **1987**, *91*, 1217–1221.
(29) McLachlan, R. D.; Carter, V. B. *Spectrochim. Acta, Part A* **1971**, *27*, 853–861.
(30) Marzocchi, M. P.; Castellucci, E. *J. Mol. Struct.* **1971**, *9*, 129–137.
(31) Emmons, E. D.; Velisavljevic, N.; Schoonover, J. R.; Dattelbaum, D. M. *Appl. Spectrosc.* **2008**, *62*, 142–148.
(32) Emmons, E. D.; Kraus, R. G.; Duvvuri, S. S.; Thompson, J. S.; Covington, A. M. *J. Polym. Sci., Part B: Polym. Phys.* **2007**, *45*, 358–367.
(33) Kraus, R. G.; Emmons, E. D.; Thompson, J. S.; Covington, A. M. *J. Polym. Sci., Part B: Polym. Phys.* **2008**, *46*, 734–742.
(34) Chellappa, R. S.; Chandra, D.; Gramsch, S. A.; Hemley, R. J.; Lin, J. F.; Song, Y. *J. Phys. Chem. B* **2006**, *110*, 11088–11097.

JP9092892